Three-dimensional Dirac semimetal and quantum transport in Cd_3As_2

Zhijun Wang, Hongming Weng,* Quansheng Wu, Xi Dai, and Zhong Fang†
Beijing National Laboratory for Condensed Matter Physics, and Institute of Physics, Chinese Academy of Sciences, Beijing 100190, China
(Received 29 May 2013; revised manuscript received 5 September 2013; published 23 September 2013)

Based on the first-principles calculations, we recover the silent topological nature of Cd_3As_2, a well known semiconductor with high carrier mobility. We find that it is a symmetry-protected topological semimetal with a single pair of three-dimensional (3D) Dirac points in the bulk and nontrivial Fermi arcs on the surfaces. It can be driven into a topological insulator and a Weyl semimetal state by symmetry breaking, or into a quantum spin Hall insulator with a gap more than 100 meV by reducing dimensionality. We propose that the 3D Dirac cones in the bulk of Cd_3As_2 can support sizable linear quantum magnetoresistance even up to room temperature.

DOI: 10.1103/PhysRevB.88.125427 PACS number(s): 73.43.−f, 71.20.−b, 73.20.−r

I. INTRODUCTION

Weyl semimetal is a new topological state of three-dimensional (3D) quantum matters,[1–6] different from the 3D topological insulators (TI).[7–9] It can be characterized by Weyl nodes (at Fermi level) in the bulk and Fermi arcs on the surfaces.[4,5] Around the Weyl nodes, the low energy physics is given as 3D two-component Weyl fermions[1,2] $H = v\vec{\sigma}\cdot\vec{k}$ (where $\vec{\sigma}$ is the Pauli matrix and $\vec{k}$ is the crystal moment), which carries chirality, left or right handed defined by the sign of velocity v. Weyl nodes are stable topological objects as long as $\vec{k}$ is well defined, and can be viewed as effective magnetic monopoles in the 3D momentum space.[3] To get Weyl semimetal, either time reversal (TR) or inversion symmetry needs to be broken.[6] Otherwise, there will be double degeneracy for all $\vec{k}$. In the case with both TR and inversion symmetries, however, we may expect a 3D Dirac semimetal state described as four-component Dirac fermions

$$H = \begin{pmatrix} v\vec{\sigma}\cdot\vec{k} & 0 \\ 0 & -v\vec{\sigma}\cdot\vec{k} \end{pmatrix},$$

which can be viewed as two copies of distinct Weyl fermions. Unfortunately, this expectation is generally not true, because two Weyl nodes with opposite chirality may annihilate each other if they overlap in momentum space, and open up a gap in general. Therefore, additional symmetry is required to protect the 3D Dirac semimetal[10–12] state and to prohibit the possible mass term, unless it is at the phase boundary between TI and normal insulators,[13] a subtle situation hard to be controlled.

The symmetry protected 3D Dirac semimetal has been discussed[10,11] for systems with spin-orbit coupling (SOC), focusing on special $\vec{k}$ points with four-dimensional-irreducible representation (FDIR),[10] which usually appears at the Brillouin zone (BZ) boundary with nonsymmorphic double space groups. In general, this FDIR requirement is too strong, and we may expect much wider compound choices by considering two doubly degenerate bands with distinct 2D representations and unavoidable band crossing (protected by crystalline symmetry). In such a case we may get 3D Dirac points along the high-symmetry lines rather than high-symmetry points at the BZ boundary. This scenario of Dirac semimetal has been suggested in our earlier studies on Na_3Bi,[12] which is unfortunately not stable in air. In this paper we show that a well known compound Cd_3As_2 is a symmetry-protected 3D Dirac semimetal with a single pair of Dirac points in the bulk and nontrivial Fermi arcs on the surface. It can be driven into a topological insulator, a Weyl semimetal, or a quantum spin Hall (QSH) insulator with a gap more than 100 meV. It can also support sizable linear quantum magnetoresistance (MR) even up to room temperature. The nice aspect of Cd_3As_2 is the high carrier mobility up to 1.5 $m^2\ V^{-1}\ s^{-1}$ at room temperature and 8.0 $m^2\ V^{-1}\ s^{-1}$ at 4 K, reported about 50 years ago.[14] This makes it a promising candidate for future transport studies. We will start from the structure and methods in Sec. II, present the main results in Sec. III, and finally conclude in Sec. IV.

II. CRYSTAL STRUCTURE AND METHODOLOGY

Among the II_3-V_2-types narrow gap semiconductors, Cd_3As_2 has drawn crucial attention, because it was believed to have inverted band structure,[15,16] whereas all others Cd_3P_2, Zn_3As_2, and Zn_3P_2 have normal band ordering. In contrast to other inverted band compounds (like HgTe, HgSe, and α-Sn), Cd_3As_2 belongs to tetragonal symmetry, and is the representative of this group, which has the splitted valence band top at $\vec{k} = 0$. The crystal structure of Cd_3As_2 is complicated, and can be related to tetragonally distorted antifluorite structure with 1/4 Cd site vacancy. If the distribution of these vacancies is random, one may treat it by virtual crystal approximation (VCA) for simplicity.[17,18] However, those vacancies are in fact ordered even at room temperature, leading to a tetragonal structure with D_{4h}^{15} ($P4_2/nmc$) symmetry (40 atoms per unit cell, called structure I hereafter), or a body centered tetragonal structure with C_{4v}^{12} ($I4_1cd$) symmetry (80 atoms per unit cell, called structure II hereafter), with the later structure more favored.[19] This vacancy ordering and very large cell of Cd_3As_2 cause historically serious problems for theoretical studies, and there is no existing first-principles calculations up to now. We report here band-structure calculations of Cd_3As_2 with its true structures and with SOC included.

We perform the first-principles band-structure calculations within the density functional formalism as implemented in VASP,[20] and use the all-electron projector augmented wave (PAW)[21] basis sets with the generalized gradient approximation (GGA) of Perdew, Burke, and Ernzerhof (PBE)[22] for the exchange correlation potential. The Hamiltonian contains the scalar relativistic corrections, and the spin-orbit coupling is taken into account by the second variation method.[23] The

 ©2013 American Physical Society

cutoff energy for the plane wave expansion was 500 eV and a **k**-point mesh of $10 \times 10 \times 6$ and $6 \times 6 \times 6$ are used for the bulk calculations of structures I and II, respectively.

For the convenience of our later discussions for the effective low energy physics, here we briefly introduce our modified second-order eight-band Kane model[24] for typical semiconductors. We start from the standard four-band second-order Kane model[24] for the case of without SOC, and then introduce additional terms to take into account the particular tetragonal symmetry of Cd_3As_2. In the $k \cdot p$ approximation, considering the low energy $|s\rangle, |p_x\rangle, |p_y\rangle, |p_z\rangle$ states (as basis) around Γ, the modified four-band Kane model is given as

$$H_4(\vec{k}) = \begin{pmatrix} A'\vec{k}^2 + E_s & ik_xP & ik_yP & ik_zP + d \\ -ik_xP & Lk_x^2 + M\left(k_y^2 + k_z^2\right) + E_p & Nk_xk_y & Nk_xk_z \\ -ik_yP & Nk_xk_y & Lk_y^2 + M\left(k_x^2 + k_z^2\right) + E_p & Nk_yk_z \\ -ik_zP + d & Nk_xk_z & Nk_yk_z & Lk_z^2 + M\left(k_x^2 + k_y^2\right) + E_p - \delta \end{pmatrix}$$

comparing with the standard isotropic four-band Kane model,[24] here we consider the anisotropic tetragonal symmetry, and introduce the paramter δ for the crystal-field splitting of $|p\rangle$ orbitals. The other parameter d is introduced to describe the breaking of inversion symmetry for structure II, and it should be zero for structure I. Then our modified eight-band Kane model can be obtained by adding the SOC term as

$$H_8(\vec{k}) = \mathbf{I} \otimes H_4(\vec{k}) + H_{so},$$

$$H_{so} = \frac{\Delta}{2} \begin{pmatrix} 0 & 0 & 0 & 0 & 0 & 0 & 0 & 0 \\ 0 & 0 & -i & 0 & 0 & 0 & 0 & 1 \\ 0 & i & 0 & 0 & 0 & 0 & 0 & -i \\ 0 & 0 & 0 & 0 & 0 & -1 & i & 0 \\ 0 & 0 & 0 & 0 & 0 & 0 & 0 & 0 \\ 0 & 0 & 0 & -1 & 0 & 0 & i & 0 \\ 0 & 0 & 0 & -i & 0 & -i & 0 & 0 \\ 0 & 1 & i & 0 & 0 & 0 & 0 & 0 \end{pmatrix},$$

where **I** is the 2×2 identity matrix and Δ denotes the strength of SOC.

III. RESULTS AND DISCUSSIONS

A. Electronic structures and band inversion

Similar to most of the semiconductors with antifluorite or zinc-blende structures, the low energy electronic properties of Cd_3As_2 are mostly determined by the Cd-5s states (conduction bands) and the As-4p states (valence bands), as shown in Fig. 1. However, there are two distinct features: (1) band inversion around the Γ point with the s state (red solid cycle) lower than the p states, which is an important sign of nontrivial topology; (2) semimetallic with band crossing along the Γ-Z direction. This band crossing is unavoidable, because the two bands belong to different (Λ_6 and Λ_7) representations, respectively, as distinguished by C_4 rotational symmetry around the k_z axis. The different representation prohibits hybridization between them, resulting in the protected band crossing. Furthermore, the crossing points should locate exactly at the Fermi level due to a charge neutrality requirement, resulting in a 3D Dirac semimetal state with the Fermi surface consisting of a single pair of Fermi points (two symmetric points along k_z related by TR). Both structures I and II share the above common features but with one important difference: Structure I has an inversion center but structure II does not.

As had been attempted with the perturbation method,[25] vacancy ordering and BZ folding play an important role for the band inversion, in contrast to the cases of HgTe or Ag_2Te,[26] where it was driven by the the shallow d states. To prove

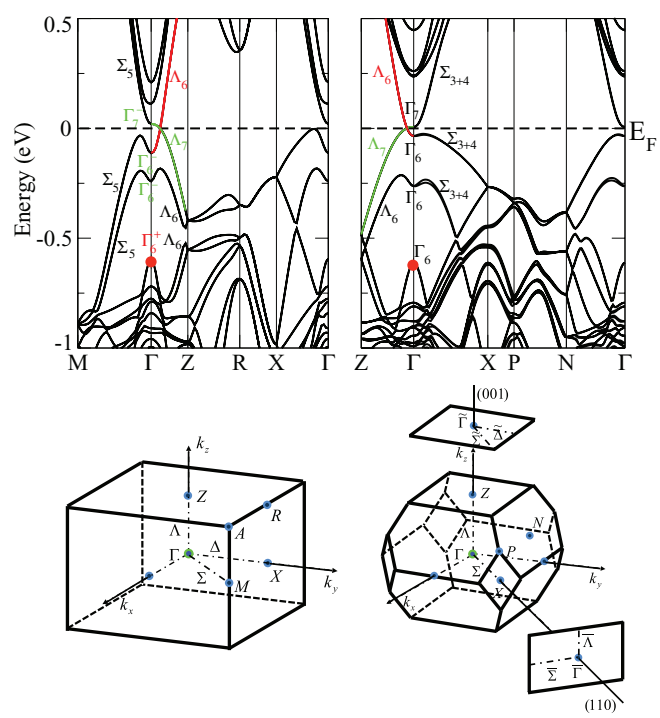

(a) structure I (b) structure II

FIG. 1. (Color online) The calculated band structures for Cd_3As_2 with crystal structure I (a) and II (b), as well as the definition of high symmetric points in each Brillouin zone (BZ). The projected surface BZ for structure II is also shown. The representation of selected bands at Γ and along high symmetric $\vec{k}$ path are indicated. Solid dots in band structures indicate the projected s bands.

TABLE I. The fitted parameters for the eight-band model.

E_s (eV)	E_p (eV)	δ (eV)	d (eV)	Δ (eV)
−0.610367	−0.069191	0.072439	0.027	0.16
P (eV Å)	A' (eV Å^2)	L (eV Å^2)	M (eV Å^2)	N (eV Å^2)
6.302242	8.013873	−5.675600	−7.957689	−10.757965

this, we performed calculations for Cd_3As_2 in hypothetic antifluorite structure without vacancy (using VCA) and in cubic antifluorite structure with one Cd vacancy, keeping the same lattice constant. We found that the former (later) has normal (inverted) band ordering at Γ. At the BZ boundary X point of hypothetic antifluorite structure without vacancy, there exist shallow s and p states, which are folded onto the Γ point of real structure. Therefore, the hybridization among the states with the same representation will push the states away from each other, i.e., make the lowest s state lower and the highest p state higher, resulting in the band inversion at Γ. The band inversion calculated from GGA is about 0.7 eV for both structures I and II. Considering the possible underestimation of GGA for the s-p gap, we have improved the calculations by HSE method,[27] and still found the band inversion around 0.3 eV, being consistent with most of the existing experimental evidence, such as the optical and transport measurements.[15]

The calculated band structures of Cd_3As_2 can be well fitted by using our modified eight-band Kane model presented in the previous section, and the obtained parameters are listed in Table I.

B. Minimal effective Hamiltonian for the 3D Dirac fermion

The atomic Cd-5s and As-4p states with SOC can be written as the states with definite angular momentum J and J_z, i.e., $|S_{J=\frac{1}{2}}, J_z = \pm\frac{1}{2}\rangle$, $|P_{\frac{3}{2}}, \pm\frac{3}{2}\rangle$, $|P_{\frac{3}{2}}, \pm\frac{1}{2}\rangle$, $|P_{\frac{1}{2}}, \pm\frac{1}{2}\rangle$. In the tetragonal crystal symmetry, however, the total angular momentum J is no longer a good quantum number, and the valence p states have complete splitting at Γ. The heavy-hole p state $\Gamma_7 = |P_{\frac{3}{2}}, \pm\frac{3}{2}\rangle$ and the conduction s state $\Gamma_6 = |S_{\frac{1}{2}}, \pm\frac{1}{2}\rangle$ remain to be the eigenstates at Γ, while the light-hole states $|P_{\frac{3}{2}}, \pm\frac{1}{2}\rangle$ can mix with the split-off state $|P_{\frac{1}{2}}, \pm\frac{1}{2}\rangle$, forming two new eigenstates which are irrelevant to the low energy physics here.

The band inversion nature of Cd_3As_2 around the Γ can be caught by considering only the minimal basis set of $|S_{\frac{1}{2}}, \frac{1}{2}\rangle$, $|P_{\frac{3}{2}}, \frac{3}{2}\rangle$, $|S_{\frac{1}{2}}, -\frac{1}{2}\rangle$, and $|P_{\frac{3}{2}}, -\frac{3}{2}\rangle$ states. To describe the 3D Dirac fermion, an effective low energy Hamiltonian $H_\Gamma(\vec{k})$ can therefore be obtained by downfolding the eight-band model into the subspace spanned by the four minimal basis. The resulting $H_\Gamma(\vec{k})$ reads

$$H_\Gamma(\vec{k}) = \epsilon_0(\vec{k}) + \begin{pmatrix} M(\vec{k}) & Ak_+ & Dk_- & B^*(\vec{k}) \\ Ak_- & -M(\vec{k}) & B^*(\vec{k}) & 0 \\ Dk_+ & B(\vec{k}) & M(\vec{k}) & -Ak_- \\ B(\vec{k}) & 0 & -Ak_+ & -M(\vec{k}) \end{pmatrix},$$

where $\epsilon_0(\vec{k}) = C_0 + C_1k_z^2 + C_2(k_x^2 + k_y^2)$, $k_\pm = k_x \pm ik_y$, and $M(\vec{k}) = M_0 - M_1k_z^2 - M_2(k_x^2 + k_y^2)$ with parameters M_0, M_1, $M_2 < 0$ to reproduce band inversion. Under the tetragonal symmetry, the leading-order term of $B(\vec{k})$ has to take the high-order form of $(\alpha k_z + \beta D)k_+^2$, which can be neglected if we only consider the expansion up to $O(k^2)$. The terms containing D describe the breaking of inversion symmetry, which should be zero for structure I. In such a case the energy dispersion is $E(\vec{k}) = \epsilon_0(\vec{k}) \pm \sqrt{M(\vec{k})^2 + A^2k_+k_-}$, having a pair of fourfold degenerate zero energy Dirac points at $\vec{k}^c = (0,0,k_z^c = \pm\sqrt{\frac{M_0}{M_1}})$. Around the neighborhood of each Dirac point, we can further expand the Hamiltonian up to $O(k^2)$. The resulting Hamiltonian is nothing but the one for 3D massless Dirac fermions, which has anisotropic linear dispersion $\Delta E(\vec{k}^c + \delta\vec{k}) \approx \pm|\delta\vec{k}| = \sqrt{(A\delta k_x)^2 + (A\delta k_y)^2 + (2M_1k_z^c\delta k_z)^2}$ (where $\delta\vec{k}$ is the deviation of momentum $\vec{k}$ from the Dirac point $\vec{k}^c$). The block diagonal form allows us to decouple the 4×4 matrix into two 2×2 matrices, which are Weyl fermions with degenerate energy but opposite chirality. For structure II, which has no inversion symmetry, the nonvanishing D term will modify the in-plane velocity from A to $A \pm \frac{1}{2}D$, while keep the Weyl nodes degenerate (because the C_{4v} symmetry along the Γ-Z axis contains only 2D irreducible representations for its double space group). The resulting Dirac semimetal state has fourfold degenerate Dirac points, but with splitting of in-plane band dispersions away from Dirac points (Fig. 2). This is a new type of 3D Dirac semimetal state, in contrast to other examples.[10,12]

A stable Weyl semimetal state with two Weyl nodes separated in momentum space can be introduced either by lowering the crystal symmetry from C_{4v} to C_4, or by breaking the TR symmetry.[12] In particular, due to the large g factor (around 30–40) of Cd_3As_2,[28] an exchange-splitting of ∼2 meV can be introduced by moderate 1 T magnetic field (if we neglect the orbital effects). On the other hand, if the fourfold rotational symmetry is broken, a linear leading order term of $B(\vec{k}) \approx B_1k_z$ will be introduced in the effective Hamiltonian H_Γ. In such a case two Weyl nodes will be coupled together, resulting in massive Dirac fermions with a gap opening. We have checked the topological invariant Z_2 number for this resulting insulating state, and found it is odd, confirming that

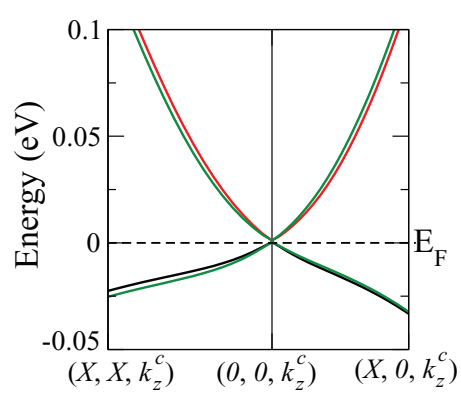

FIG. 2. (Color online) Band dispersions and band splitting in the plane passing through Dirac point (0,0,k_z^c) and perpendicular to Γ-Z for structure II. The k points are indicated in cartesian coordinates. X and k_z^c are around 0.1 and 0.032 Å^{-1}, respectively.

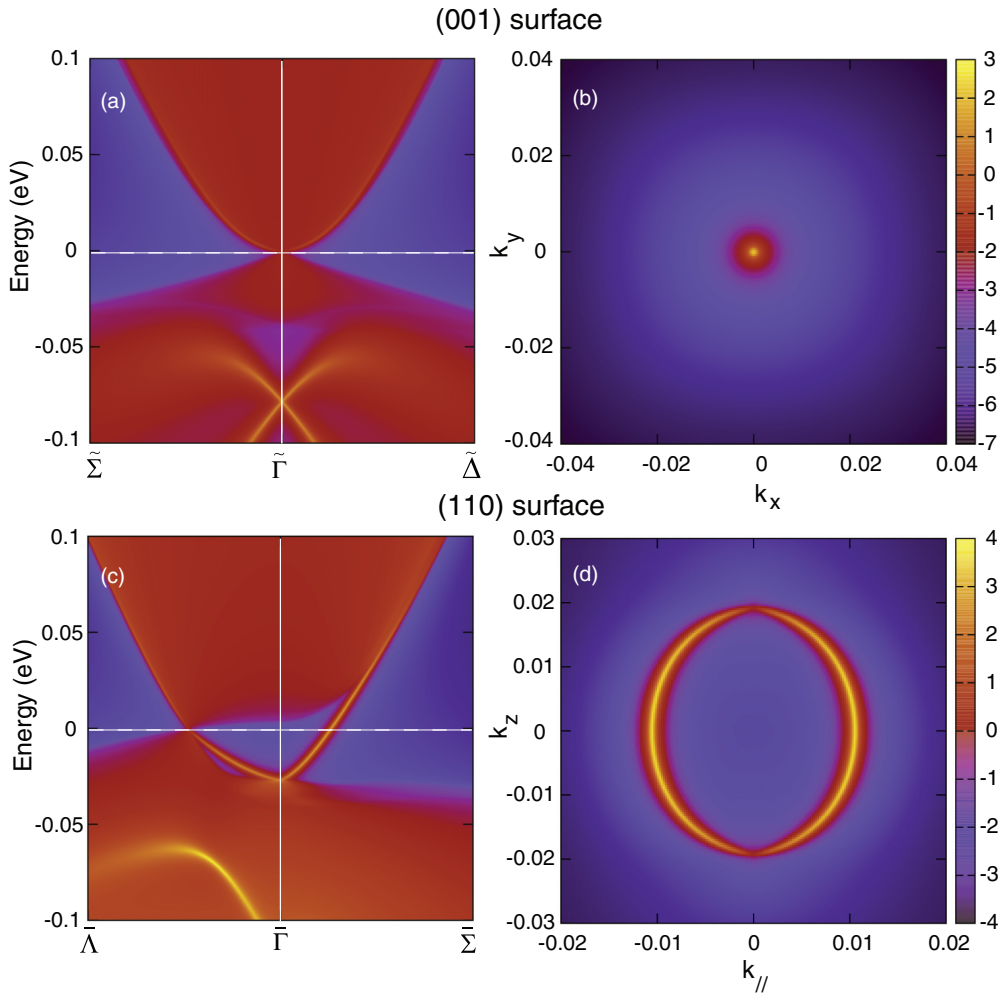

FIG. 3. (Color online) The calculated surface states (left panels) and corresponding Fermi surface (right panels) of structure II Cd_3As_2 for its (001) (upper panels) and (110) (lower panels) surface.

it is a 3D topological insulator[7,8] (due to the inverted band structure).

C. Surface states and quantum transport properties

The nontrivial topology and the 3D Dirac cones in Cd_3As_2 suggest the presence of nontrivial surface states. For this purpose, we transform the eight-band model into a tight-binding model on a tetragonal lattice by introducing the substitutions:

$$k_i \to \frac{1}{L_i}\sin(k_i L_i),$$
$$k_i^2 \to \frac{2}{L_i^2}[1-\cos(k_i L_i)](L_{x,y}=a,\ L_z=c).$$

Here k_i refers to k_x, k_y, and k_z, while a and c are the tetragonal lattice constants, which are taken as 3.0 and 5.0 Å, respectively. This approximation is valid in the vicinity of the Γ point. We use an iterative method to obtain the surface Green's function of the semi-infinite system.[29] The imaginary part of the surface Green's function is the local density of states (LDOS) at the surface. Since GGA underestimate the s-p band gap by about 0.4 eV as discussed above, we have artificially lifted the on-site energy of the s state (as given in Table I) by 0.4 eV in the surface state calculations.

The obtained LDOS on semi-infinite (001) and (110) surfaces of structure II are presented in Fig. 3. For the (001) surface, the surface projection of continuous bulk states superposes the nontrivial surface states, and its Fermi surface is just a point [Fig. 3(b)]. For the (110) surface, however, the nontrivial surface states are clearly visible. Its Fermi surface is composed of two half-circle Fermi arcs, touching at the singularity points ($k_\parallel = 0$, $\pm k_z^c$) where the surface projection of bulk Dirac points exist.

The existence of 3D Dirac cones in the bulk also implies that we can expect the QSH effect if we reduce the dimensionality and form the quantum-well structure of Cd_3As_2. This provides an alternative compound choice to the existing experiments,[30,31] which all require extreme conditions up to now. The band structure of z-oriented Cd_3As_2 thin film of different thickness can be understood as the bulk bands in different k_z-fixed planes. The 2D Z_2 number can be nonzero only for limited regions where the band inversion happens when going from Γ to Z. In the quantum-well structure, those low energy states around Γ should be further quantized into subbands, whose energy levels change as a function of film

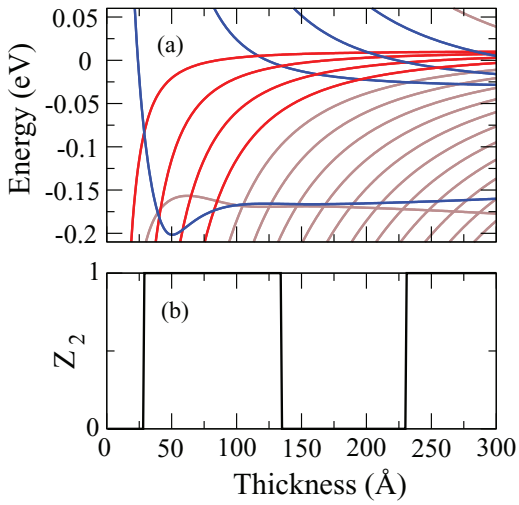

FIG. 4. (Color online) The thickness dependence of (a) subband energies and (b) Z_2 number of z-oriented quantum well of Cd_3As_2.

thickness [Fig. 4(a)]. When the thickness of the film is thin enough, the band inversion in the bulk band structure will be removed entirely by the finite size effect. With the increment of the film thickness, the finite size effect is getting weaker and the band inversion among these subbands restores subsequently, which leads to jumps in the Z_2 number. Then, depending on the number of band inversions associated with the subbands, the system should cross over between trivial and nontrivial 2D insulators oscillatorily as a function of thickness[32] [Fig. 4(b)]. Comparing with the HgTe/CdTe quantum well,[30] the first critical thickness of Cd_3As_2 is much thinner (2.9 vs 6.3 nm), suggesting possibly a larger gap. To be a concrete example, a 5 nm thick Cd_3As_2 film is a good QSH insulator with a gap more than 100 meV. Given the known high mobility of Cd_3As_2, it is therefore a good candidate for the QSH measurement.

Finally, we propose that crystalline Cd_3As_2 with 3D Dirac cone is an ideal system to check Abrikosov's proposal of quantum MR,[33] and may support sizable linear MR even up to room temperature. Quantum effects become noticeable when the individual Landau levels are distinct: $\hbar\omega_c > k_B T$. The Dirac system has a linear energy spectrum, and its cyclotron frequency ω_c should follow the square root rule ($\omega_c = v\sqrt{eB/c}$), in contrast with nonrelativistic system where ω_c is linear in field B. Using calculated velocity $v = 3 \times 10^7$ cm/s for Cd_3As_2, this then leads to $\hbar\omega_c \sim 280$ K for $B = 10$ T. The linear quantum MR can be estimated[33] as $\Delta\rho(B)/\rho(0) = N_i B/\pi n^2 ec\rho(0) = N_i B\mu/\pi nc$ (where $\rho(0) = 1/ne\mu$ is used, n is the carrier density, μ is mobility, and N_i is the density of the scattering centers). Taking the experimental values $\mu \sim 1.5$ m^2 V^{-1} s^{-1} at room temperature, and assuming n and N_i are in the same order, MR ratio can reach 50% per 1 T field. If the scattering is not phonon mediated, we expect that N_i is not sensitive to temperature, then MR is mostly determined by n and μ, which should lead to even enhanced MR at lower temperature.

IV. CONCLUSION

In summary, based on the first-principles calculations and effective model analysis, we have shown that the known compound Cd_3As_2 is a symmetry-protected topological semimetal with a pair of 3D Dirac points (located at the Fermi level) in the bulk and Fermi arcs on the surfaces. It can be driven into various topologically distinct phases, such as topological insulator and Weyl semimetal state by symmetry breakings. In addition, due to its unique 3D Dirac cone type electronic structure, we can expect the QSH effect in its quantum-well structure and the sizable linear quantum MR even up to the room temperature. It will be of particular interest, in such a 3D topological semimetal, to see whether the superconductivity can be achieved by carrier doping or not, because such a superconducting state if obtained may be related to the topological superconductivity.[34]

ACKNOWLEDGMENTS

The first-principles calculations are performed by using the computers in the Nation Supercomputer Center in Tianjin of China. We acknowledge the support from NSF of China and the 973 program of China (No. 2011CBA00108 and No. 2013CBP21700).

*hmweng@aphy.iphy.ac.cn
†zfang@aphy.iphy.ac.cn

[1] H. Weyl, Z. Phys. **56**, 330 (1929).
[2] G. T. Volovik, JETP Lett. **75**, 55 (2002).
[3] Z. Fang, N. Nagaosa, K. S. Takahashi *et al.*, Science **302**, 92 (2003).
[4] X. G. Wan, A. M. Turner, A. Vishwanath, and S. Y. Savrasov, Phys. Rev. B **83**, 205101 (2011).
[5] G. Xu, H. M. Weng, Z. J. Wang, X. Dai, and Z. Fang, Phys. Rev. Lett. **107**, 186806 (2011).
[6] A. A. Burkov and L. Balents, Phys. Rev. Lett. **107**, 127205 (2011); A. A. Burkov, M. D. Hook, and L. Balents, Phys. Rev. B **84**, 235126 (2011); G. B. Halász and L. Balents, *ibid.* **85**, 035103 (2012).
[7] M. Z. Hasan and C. L. Kane, Rev. Mod. Phys. **82**, 3045 (2010).
[8] X.-L. Qi and S.-C. Zhang, Rev. Mod. Phys. **83**, 1057 (2011).
[9] H. J. Zhang *et al.*, Nat. Phys. **5**, 438 (2009); Y. Xia *et al.*, *ibid.* **5**, 398 (2009); Y. L. Chen *et al.*, Science **325**, 178 (2009).
[10] S. M. Young, S. Zaheer, J. C. Y. Teo, C. L. Kane, E. J. Mele, and A. M. Rappe, Phys. Rev. Lett. **108**, 140405 (2012).
[11] J. L. Mañes, Phys. Rev. B **85**, 155118 (2012).
[12] Z. J. Wang, Y. Sun, X. Q. Chen, C. Franchini, G. Xu, H. M. Weng, X. Dai, and Z. Fang, Phys. Rev. B **85**, 195320 (2012).
[13] S. Murakami, New J. Phys. **9**, 356 (2007).
[14] See, W. Zdanowicz and L. Zdanowicz, Annu. Rev. Mater. Sci. **5**, 301 (1975), and references therein.
[15] M. J. Aubin, L. G. Caron, and J.-P. Jay-Gerin, Phys. Rev. B **15**, 3872 (1977); L. G. Caron, J.-P. Jay-Gerin, and M. J. Aubin, *ibid.* **15**, 3879 (1977).

[16]B. Dowgiałło-Plenkiewicz and P. Plenkiewicz, Phys. Status Solidi (b) **94**, K57 (1979); G. Chuiko, N. Don *et al.*, Moldavian J. Phys. Sci. **2**, N1.88 (2003).
[17]P. J. Lin-Chung, Phys. Rev. **188**, 1272 (1969).
[18]K. Sieranski, J. Szatkowski, and J. Misiewicz, Phys. Rev. B **50**, 7331 (1994).
[19]G. A. Steigmann and J. Goodyear, Acta Cryst. **B24**, 1062 (1968).
[20]G. Kresse and J. Hafner, Phys. Rev. B **48**, 13115 (1993); G. Kresse and J. Furthmüller, Comput. Mater. Sci. **6**, 15 (1993).
[21]P. E. Blöchl, Phys. Rev. B **50**, 17953 (1994); G. Kresse and D. Joubert, *ibid.* **59**, 1758 (1999).
[22]J. P. Perdew, K. Burke, and M. Ernzerhof, Phys. Rev. Lett. **77**, 3865 (1996).
[23]D. D. Koelling and B. N. Harmon, J. Phys. C: Solid State Phys. **10**, 3107 (1977).
[24]L. C. Lew Yan Voon and M. Willatzen, *The k·p Method: Electronic Properties of Semiconductors* (Springer, Berlin, 2009). See pp. 59–60 for the definition of parameters and four-bands Kane model.
[25]B. Plenkiewicz, P. R. Wallace, and P. Plenkiewicz, Solid State Commun. **50**, 681 (1984).
[26]W. Zhang, R. Yu, W. Feng, Y. Yao, H. M. Weng, X. Dai, and Z. Fang, Phys. Rev. Lett. **106**, 156808 (2011).
[27]J. Heyd, G. Scuseria, and M. Ernzerhof, J. Chem. Phys. **118**, 8207 (2003).
[28]J. Bodnar, *Proceedings of the 3rd International Conference on Physics of Narrow-Gap Semiconductors* (PWN, Warsaw, 1978), p. 311; P. R. Wallace, Phys. Status Solidi (b) **92**, 49 (1979).
[29]W. Zhang, R. Yu, H. J. Zhang, X. Dai, and Z. Fang, New J. Phys. **12**, 065013 (2010).
[30]M. Kónig, S. Wiedmann, C. Brune, A. Roth, H. Buhmann, L. W. Molenkamp, X.-L. Qi, and S.-C. Zhang, Science **318**, 766 (2007).
[31]C. X. Liu, T. L. Hughes, X. L. Qi, K. Wang, and S.-C. Zhang, Phys. Rev. Lett. **100**, 236601 (2008); I. Knez, R. R. Du, and G. Sullivan, *ibid.* **107**, 136603 (2011).
[32]C. X. Liu, H. J. Zhang, B. H. Yan, X. L. Qi, T. Frauenheim, X. Dai, Z. Fang, and S. C. Zhang, Phys. Rev. B **81**, 041307 (2010).
[33]A. A. Abrikosov, Phys. Rev. B **58**, 2788 (1998).
[34]X. L. Qi, T. L. Hughes, and S. C. Zhang, Phys. Rev. B **81**, 134508 (2010).